Velocity continuation by finite differences

A. Novais*, J. Costa†, and R. Portugal**

*Dept. of Applied Math., IMECC-UNICAMP, CP 6065, 13081-970 Campinas (SP), Brazil

**Geophysical Institute, UNICAMP, 13081-970 Campinas (SP), Brazil

†Geophysical Institute, University of Pará, 66.075-110, Belém (PA), Brazil

This paper was prepared for presentation at the 9th International Congress of The Brazilian Geophysical Society held in Salvador, Brazil, 11-14 September 2005.

Abstract

We have implemented a finite-difference algorithm for time-remigration of GPR data in FORTRAN 90 and C, and studied its theoretical properties in detail. For a number of synthetic models, out numerical experiments have been realized. For these examples, we obtained perfect agreement between the theoretical predictions and numerical results. The examples also prove the computational efficiency of the algorithm. Estimates of the true medium velocity can be obtained.

Introduction

The objective of this work is the construction of an image of the geological structure of the underground using recordings of seismic waves that have propagated through this medium. This image construction is generally known as migration. An update of the migrated image, which might turn out to be necessary, for example, if the image was obtained using an incorrect velocity model and an improved model has become available, is often referred to as remigration.

To construct a seismic image from GPR sections, it is necessary to carry out a migration. This process repositions the reflectors and collapses the diffractions, in this way generating an image that actually represents the geometry of the reflecting interfaces in the underground. For a successful application of a seismic migration, the knowledge of the velocity distribution in the underground is essential. In this work, we demonstrate the implementation of a strategy to carry out repeated migrations in a very fast way, each for a different velocity value. The permitted values for the migration velocity can vary in a user-defined range. The result of this process is a sequence of images that can be evaluated by the interpreter. In this way, he can choose that particular image and migration velocity which best satisfies his given interpretive criteria.

The necessity to improve a given migrated image is frequent in seismic and GPR applications. The reason is that the correct velocity model is unknown and has to be determined during the process of constructing the best possible image. In conventional seismic processing, the estimation of a velocity model is carried out by constructing velocity panels from CMP gathers using different offsets. However, this is not a common procedure in GPR processing.

This work is based on the velocity-continuation procedure as proposed by Fomel (1994) (see also Hubral et al., 1996; Fomel, 2003a,b). We have implemented a finite-difference algorithm in FORTRAN 90 and C, and studied its theoretical properties in detail. For a number of synthetic models, out numerical experiments have been realized. For these examples, we obtained perfect agreement between the theoretical predictions and numerical results. The examples also prove the computational efficiency of the algorithm.

Continuation equation

In this section, we present the method of velocity continuation for a pressure field that obeys the acoustic wave equation in a medium with constant density. All our theoretical results and numerical algorithms can be directly applied to GPR data.

When ignoring amplitude effects, the process of velocity continuation for zero-offset data can be described by the partial differential equation (Fomel, 1994; Hubral et al., 1996; Fomel, 2003a,b; Claerbout, 1986)

$$\frac{\partial^2 P}{\partial v \partial t} + vt\frac{\partial^2 P}{\partial x^2} = 0, \tag{1}$$

where $P = P(x, t, v)$ is the zero-offset section that is to be remigrated in velocity v, t is the vertical time and x is the coordinate of the midpoint between the source and the receiver. Each section of constant velocity v corresponds to one image. To solve equation (1), we need an initial and a boundary condition. The initial condition is given by the original migrated image, $P_0(x, t)$. The boundary condition can be taken from the condition that outside the migrated range, no image will be obtained. Then, the conditions read

$$P|_{t=T} = 0 \quad P|_{v=v_0} = P_0(x, t), \tag{2}$$

where v_0 is the initial velocity, and T is the boundary time. We need to choose $T = 0$ for continuations to smaller velocities and $T = t_{\max}$, i.e., the largest time value of the image, for a continuation to greater velocities.

Finite-difference approximation

We use the finite-difference method to solve the problem given by equations (1)–(2). We discretize the variables in the following way: $x_l = x_0 + l\Delta x$, $t_m = t_0 + m\Delta t$ e $v_n = v_0 + n\Delta v$, where x_0, t_0 and v_0 are the initial midpoint,

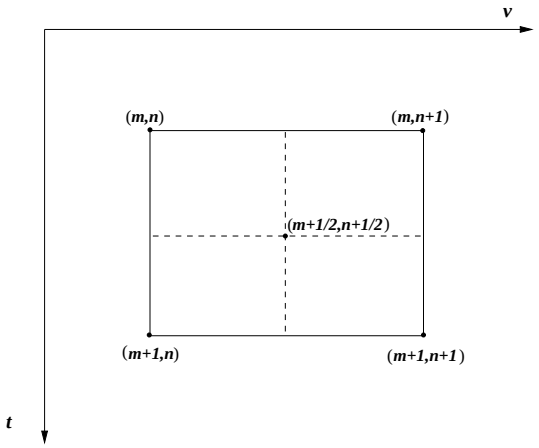

Figure 1: Discretization of the second derivative at point $(x_l, t_{m+1/2}, v_{n+1/2})$.

time, and velocity value, respectively. We denote the pressure field $P(x_l, t_m, v_n)$ by $P^n_{l,m}$. We discretize the equation at the point $(x_l, t_{m+1/2}, v_{n+1/2})$, using a centered scheme for both first derivatives in the mixed-derivative term and a second-order centered scheme for the second derivative with respect to x. In this way, we have for the mixed derivative

$$\left.\frac{\partial^2 P}{\partial v \partial t}\right|_{l,m+\frac{1}{2},n+\frac{1}{2}} = \frac{P^{n+1}_{l,m+1} - P^{n+1}_{l,m} - P^{n}_{l,m+1} + P^{n}_{l,m}}{\Delta v \Delta t}. \tag{3}$$

To discretize the second term of equation (1), we use the mean value of the operator in the vertices, as indicated in Figure 1. In this way, we obtain

$$\begin{aligned} vt\left.\frac{\partial^2 P}{\partial x^2}\right|_{l,m+\frac{1}{2},n+\frac{1}{2}} = \frac{1}{4}\big(&v_n t_m \mathbf{D}_x P^n_{l,m} + v_{n+1} t_m \mathbf{D}_x P^{n+1}_{l,m} \\ &+ v_n t_{m+1} \mathbf{D}_x P^n_{l,m+1} \\ &+ v_{n+1} t_{m+1} \mathbf{D}_x P^{n+1}_{l,m+1}\big), \end{aligned} \tag{4}$$

with $\mathbf{D}_x$ being the second-order centered finite-difference operator for the second derivative with respect to x, i.e.,

$$\mathbf{D}_x P^n_{l,m} = \frac{P^n_{l+1,m} - 2P^n_{l,m} + P^n_{l-1,m}}{\Delta x^2}. \tag{5}$$

Substituting the approximations (3) and (4) in equation (1), we obtain two inconditionally stable FD schemes. The first one is forward in velocity and backward in time,

$$\begin{aligned} (1 - a^{n+1}_m \mathbf{D}_x) P^{n+1}_{l,m} = &(1 + a^{n+1}_{m+1} \mathbf{D}_x) P^{n+1}_{l,m+1} \\ &-(1 - a^{n}_{m+1} \mathbf{D}_x) P^{n}_{l,m+1} \\ &+(1 + a^{n}_{m} \mathbf{D}_x) P^{n}_{l,m}, \end{aligned} \tag{6}$$

where $a^n_m = (v_n t_m \Delta v \Delta t)/4$. The second scheme is forward in time and backward in velocity,

$$\begin{aligned} (1 - a^{n}_{m+1} \mathbf{D}_x) P^{n}_{l,m+1} = &(1 + a^{n+1}_{m+1} \mathbf{D}_x) P^{n+1}_{l,m+1} \\ &-(1 - a^{n+1}_{m} \mathbf{D}_x) P^{n+1}_{l,m} \\ &+(1 + a^{n}_{m} \mathbf{D}_x) P^{n}_{l,m}, \end{aligned} \tag{7}$$

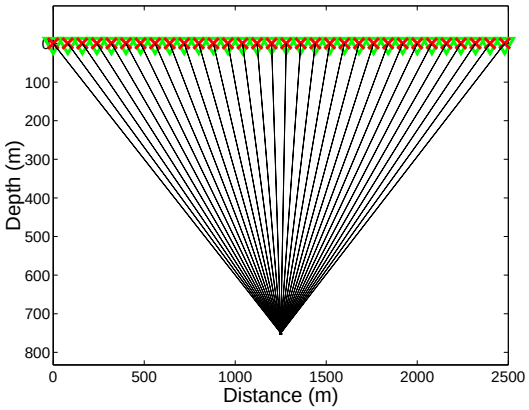

Figure 2: Model 1: Constant-velocity medium with a single diffraction point.

with the same a^n_m.

In this work, we have implemented scheme (6), which is more convenient to describe the remigration.

Numerical stability

To analyze the numerical stability of scheme (6), we utilize the von Neumann criterion (Thomas, 1995). For that purpose, we substitute $P^n_{l,m} = \xi^n \exp(i\,(l\theta_x + m\theta_t))$ in scheme (6) to obtain

$$-(a^{n+1}_m + a^{n+1}_{m+1} e^{i\theta_t})\xi = a^n_m + a^n_{m+1} e^{i\,\theta_t}. \tag{8}$$

This immediately yields

$$\xi = -\frac{a^n_m}{a^{n+1}_m}\,\frac{1 + (a^n_{m+1}/a^n_m) e^{i\,\theta_t}}{1 + (a^{n+1}_{m+1}/a^{n+1}_m) e^{i\,\theta_t}}. \tag{9}$$

Substituting the values of a^n_m in the above expression, we arrive at

$$\xi = -\frac{v_n}{v_{n+1}}. \tag{10}$$

Therefore, for increasing velocity, we have $|\xi| \leq 1$ for any grid spacing. As a consequence, this FD scheme is inconditionally stable.

To prove that also scheme (7) is inconditionally stable, it is sufficient to apply the same procedure that was used above. We conclude that the latter scheme is inconditionally stable for decreasing velocities.

Numerical experiments

Model 1:

The first model consists of a diffraction point in a horizontal position at $x = 1250$ m and depth $z = 750$ m. It is depicted in Figure 2 together with the corresponding ray family. The corresponding zero-offset section was modeled with a Ricker source pulse with a dominant frequency of 20 Hz. The true propagation medium has a velocity of 1.5 km/s (i.e., water velocity). For the zero-offset simulation, 200 source-receiver pairs were distributed along the surface symmetrically around the diffraction point, regularly space at a distance of 12.5 m. The sampling rate

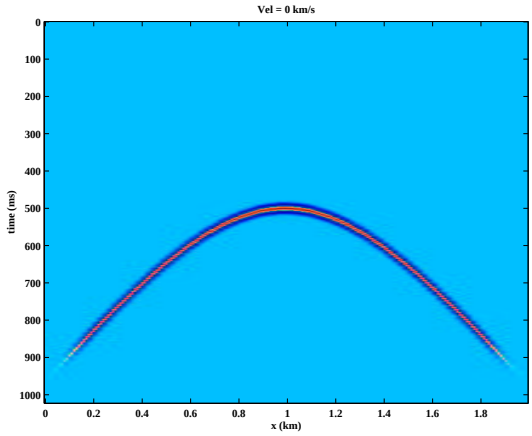

Figure 3: Zero-offset section, which corresponds to a time-migrated section with velocity 0 km/s.

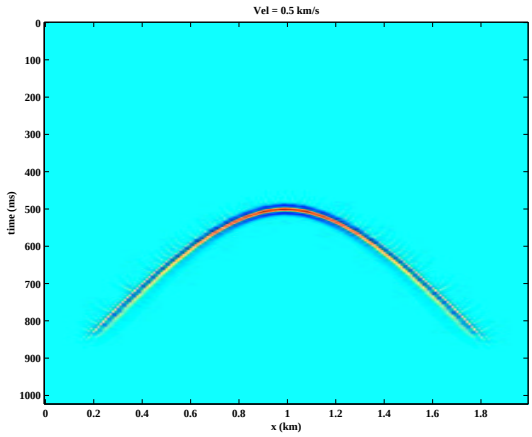

Figure 4: Remigration with velocity: 0.5 km/s

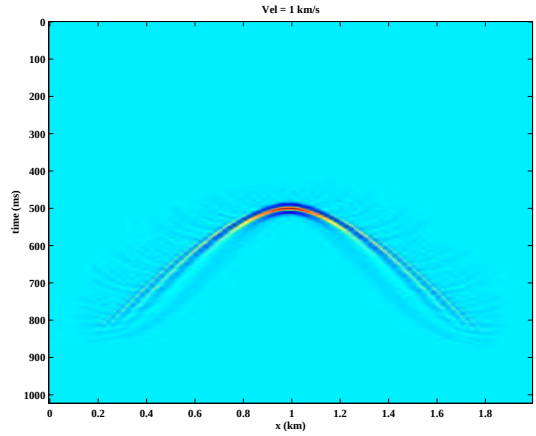

Figure 5: Remigration with velocity: 1.0 km/s

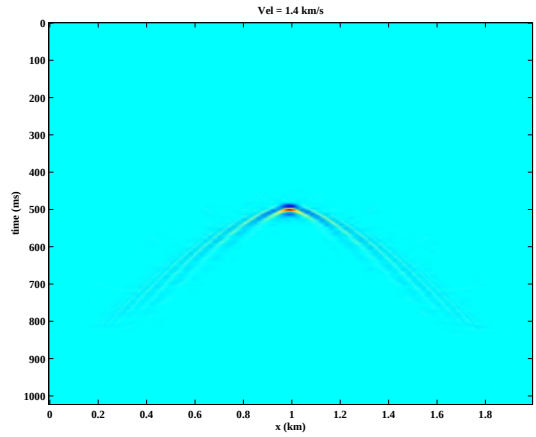

Figure 6: Remigration with velocity: 1.4 km/s

was 2 ms. Therefore, in the finite-difference computations, $\Delta x = 12.5$ m and $\Delta t = 2$ ms.

Figure 3 shows the modeled zero-offset section that corresponds to a time-migrated section with a velocity of 0 km/s. Figures 4–9 depict several remigrated sections for different values of the migration velocity. We can clearly observe the collaps of the diffraction when the migration velocity becomes equal to the true medium velocity of 1.5 km/s. Beyond this velocity, the diffraction event starts to change its shape, so that the concavity, which originally was downward, now becomes upward. For velocities greater than the true medium velocity, all migrated images have this character.

Model 2:

The second model can be seen in Figure 10. The zero-offset section is depicted in Figure 11, where the CMP spacing was chosen as 10 m. The source pulse was again a Ricker wavelet, now with a dominant frequency of 12 Hz. The true velocity of the propagation medium is 3.0 km/s, in which two reflecting interfaces are embedded. The zero-offset section was simulated using the exploding-reflector model (Lowenthal et al., 1976). Since the second reflector is a synclinal structure, the zero-offset section presents the well-known bow-tie structure. We see that as the velocity increases, the bow tie unfolds. In the section for velocity 2.8 km/s, the bow tie has already disappeared. From that velocity on, the reflector starts to smooth out. At the velocity of 3.0 km/s, it has arrived at its correct shape. As the velocity continues to increase the synclinal structe is becoming broader and broader.

Conclusions

We have shown the implementation of velocity continuation for time remigration using the finite-difference method. Through our numerical tests, we can conclude that the chosen algorithm allows to efficiently generate several migrated sections for different migration velocities. Under favorable conditions, an estimate of the best velocity can be realized by the interpreter based on the following criteria:

- If there is a diffraction event in the data, as is the case during the detection of enterred ducts, the true velocity can be determined, since at this velocity the diffraction event collapses into a single point, and for larger velocities, the concavity of the event changes.
- If there is a triplication of a reflection event in the data,

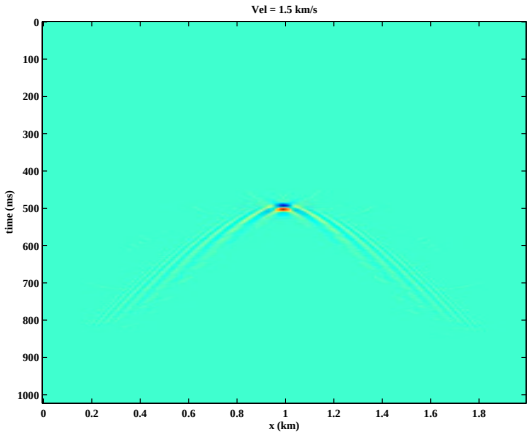

Figure 7: Remigration with velocity: 1.5 km/s

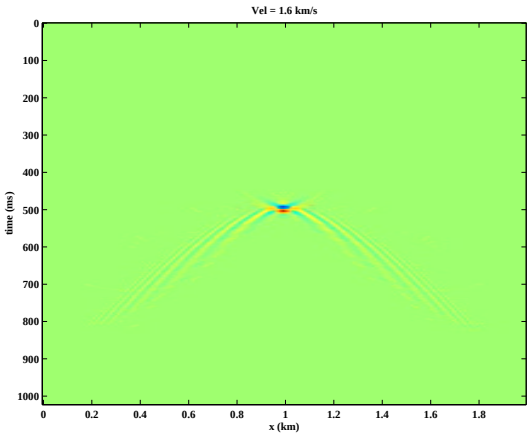

Figure 8: Remigration with velocity: 1.6 km/s

these can also be employed to estimage the correct medium velocity. At the true medium velocity, the triplication unfolds and the energy is well-distributed along the event.

- For anticlinal interfaces, an upper estimate of the true medium velocity can be found from the same criterion of the distribution of the energy along the event.

Acknowledgments

We thank the CNPq, the sponsors of the WIT Consortium and BRAIN for their financial support.

References

Claerbout, J. F., 1986, *Velocity extrapolation by cascaded 15 degree migration*, Stanford Exploration Project **SEP–48**, 79–84.

Fomel, S., 1994, Method of velocity continuation in the problem of seismic time migration: Russian Geology and Geophysics, **35**, no. 5, 100–111.

——— 2003a, Time migration velocity analysis by velocity continuation: Geophysics, **68**, 1662–1672.

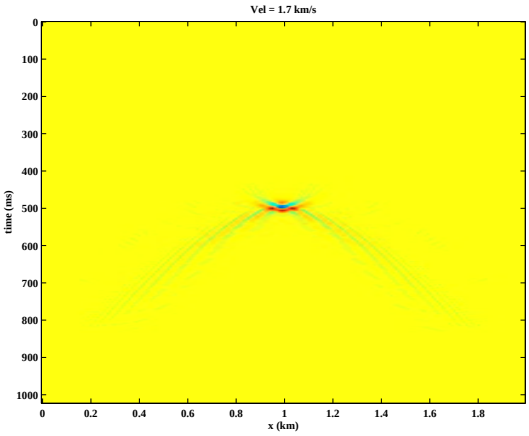

Figure 9: Remigration with velocity: 1.7 km/s

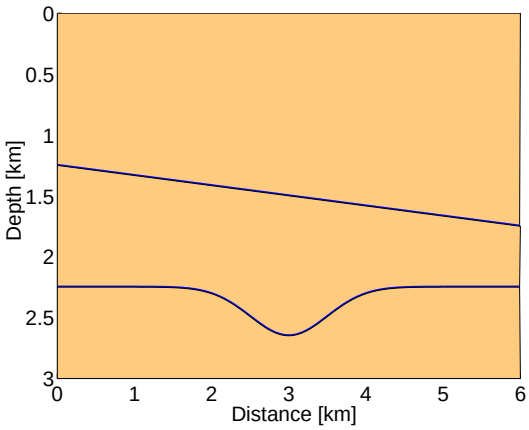

Figure 10: Model 2: Constant-velocity medium with two interfaces.

——— 2003b, Velocity continuation and the anatomy of residual prestack time migration: Geophysics, **68**, 1650–1661.

Hubral, P., M. Tygel, and J. Schleicher, 1996, Seismic image waves: Geophysical Journal International, **125**, 431–442.

Loewenthal, D., Lu, L., Roberson, R., and Sherwood, J., 1976, *The wave equation applied to migration*, Geophys. Prosp., **24**, 380 – 399.

Thomas, J. W., 1995, *Numerical Partial Differential Equations – Finite Difference Methods*, Springer Verlag, New York.

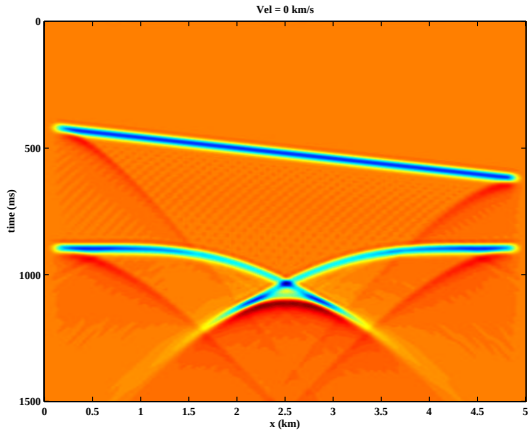

Figure 11: Zero-offset section.

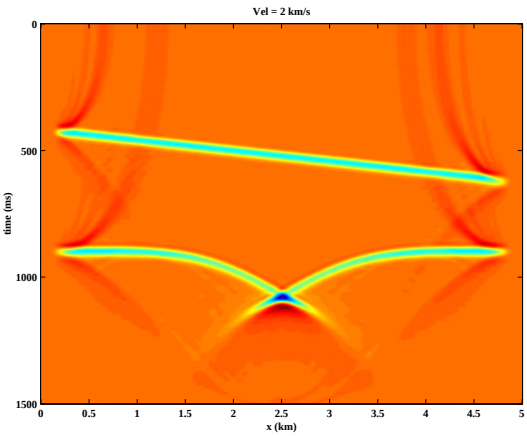

Figure 12: Remigration with velocity: 2.0 km/s

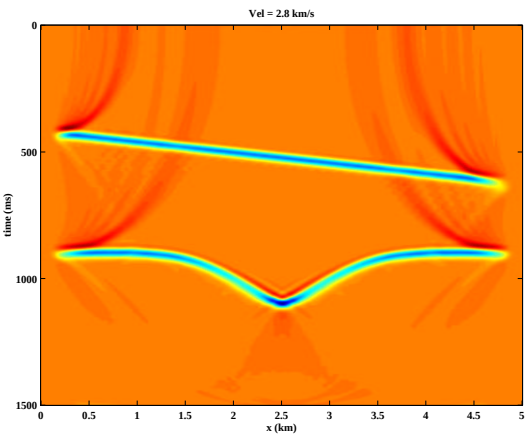

Figure 13: Remigration with velocity: 2.8 km/s

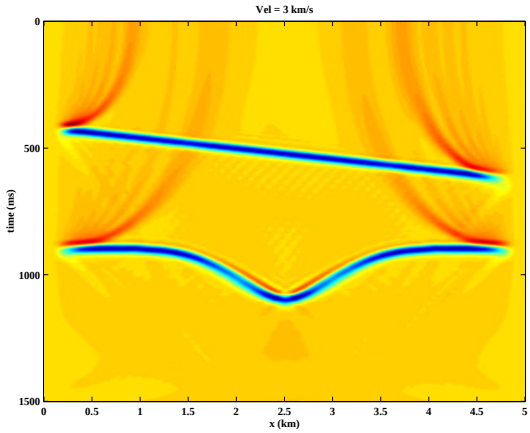

Figure 14: Remigration with velocity: 3.0 km/s

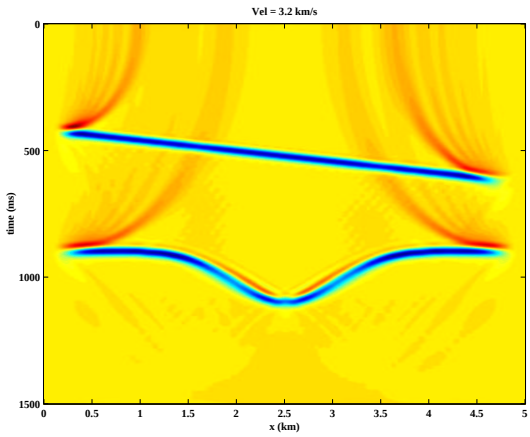

Figure 15: Remigration with velocity: 3.2 km/s

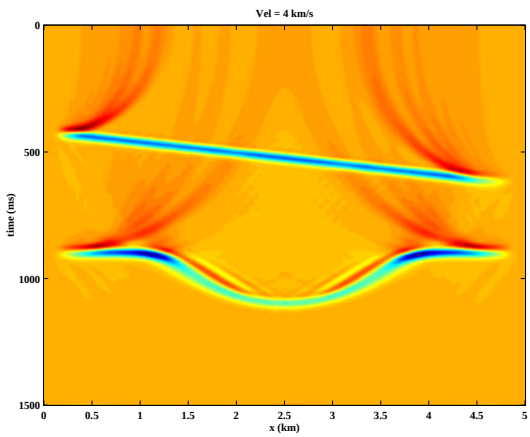

Figure 16: Remigration with velocity: 4.0 km/s